AD-A084 644 SRI INTERNATIONAL MENLO PARK CA F/G 17/9
GRADIENT SCATTERING THEORY DEMONSTRATES THAT VHF, SPREAD-F RADA--ETC(U)
NOV 78 W B CHESNUT DNA001-78-C-0075
UNCLASSIFIED DNA-4861T NL

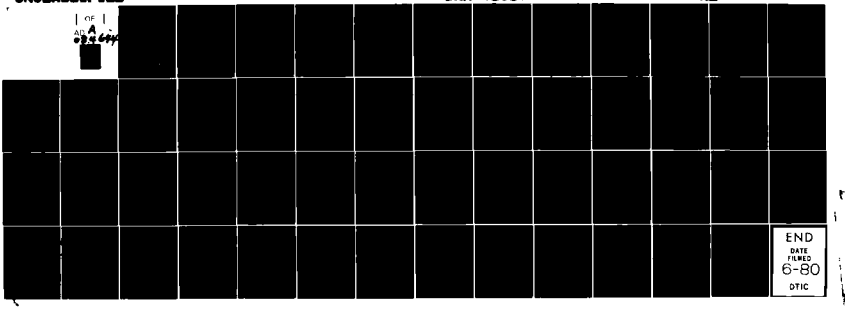

DNA 4801T

GRADIENT SCATTERING THEORY DEMONSTRATES THAT VHF, SPREAD-F RADAR BACKSCATTER REVEALS STREAMING INSTABILITIES

SRI International
333 Ravenswood Avenue
Menlo Park, California 94025

30 November 1978

Topical Report for Period January 1978—October 1978

CONTRACT No. DNA 001-78-C-0075

THIS WORK SPONSORED BY THE DEFENSE NUCLEAR AGENCY
UNDER RDT&E RMSS CODE B322078464 S99QAXHB05414 H2590D.

Prepared for
Director
DEFENSE NUCLEAR AGENCY
Washington, D. C. 20305

Destroy this report when it is no longer needed. Do not return to sender.

PLEASE NOTIFY THE DEFENSE NUCLEAR AGENCY, ATTN: STTI, WASHINGTON, D.C. 20305, IF YOUR ADDRESS IS INCORRECT, IF YOU WISH TO BE DELETED FROM THE DISTRIBUTION LIST, OR IF THE ADDRESSEE IS NO LONGER EMPLOYED BY YOUR ORGANIZATION.

UNCLASSIFIED

SECURITY CLASSIFICATION OF THIS PAGE *(When Data Entered)*

REPORT DOCUMENTATION PAGE	READ INSTRUCTIONS BEFORE COMPLETING FORM
1. REPORT NUMBER DNA 4801T	2. GOVT ACCESSION NO. AD-A084644	3. RECIPIENT'S CATALOG NUMBER
4. TITLE *(and Subtitle)* GRADIENT SCATTERING THEORY DEMONSTRATES THAT VHF, SPREAD-F RADAR BACKSCATTER REVEALS STREAMING INSTABILITIES		5. TYPE OF REPORT & PERIOD COVERED Topical Report for Period Jan 78—Oct 78
		6. PERFORMING ORG. REPORT NUMBER SRI Project 6990
7. AUTHOR(s) Walter G. Chesnut		8. CONTRACT OR GRANT NUMBER(s) DNA 001-78-C-0075
9. PERFORMING ORGANIZATION NAME AND ADDRESS SRI International 333 Ravenswood Avenue Menlo Park, California 94025		10. PROGRAM ELEMENT, PROJECT, TASK AREA & WORK UNIT NUMBERS Subtask S99QAXHB054-14
11. CONTROLLING OFFICE NAME AND ADDRESS Director Defense Nuclear Agency Washington, D.C. 20305		12. REPORT DATE 30 November 1978
		13. NUMBER OF PAGES 52
14. MONITORING AGENCY NAME & ADDRESS*(if different from Controlling Office)*		15. SECURITY CLASS *(of this report)* UNCLASSIFIED
		15a. DECLASSIFICATION DOWNGRADING SCHEDULE

16. DISTRIBUTION STATEMENT *(of this Report)*

Approved for public release; distribution unlimited.

17. DISTRIBUTION STATEMENT *(of the abstract entered in Block 20, if different from Report)*

18. SUPPLEMENTARY NOTES

This work sponsored by the Defense Nuclear Agency under RDT&E RMSS Code B322078464 S99QAXHB05414 H2590D.

19. KEY WORDS *(Continue on reverse side if necessary and identify by block number)*

Radar Scattering
Plasma Gradients
Gradient Scattering
Spread-F

20. ABSTRACT *(Continue on reverse side if necessary and identify by block number)*

Field-aligned radar backscatter echoes have been obtained from the equatorial F region using frequencies from slightly above the plasma frequency to as high as 415 MHz. In this report we study the possibility that such echoes result from steep transitions from low- to high-density plasmas. We have studied four profile forms for this transition. The first, the only physically based profile, is assumed to be associated with the gyroradius distribution of the ions in the plasma. The second profile, the Epstein

DD FORM 1 JAN 73 1473 EDITION OF 1 NOV 65 IS OBSOLETE

UNCLASSIFIED

SECURITY CLASSIFICATION OF THIS PAGE *(When Data Entered)*

20. ABSTRACT (Continued)

profile, is subject to exact reflectivity analysis and is used to provide guidance concerning the accuracy of the Born approximation used in our other calculations. The third profile, a half Gaussian wedded to a step function, a form used by Balsley and Farley, and a fourth profile, a raised cosine form, lead to very intense scattering, by hundreds of dBs, compared with that derived from our physically based gyroradius distribution. We believe we have shown that the intense scattering results computed by Balsley and Farley are due to mathematical discontinuities in the second derivatives of these last two profiles. As a result, we argue that the half-Gaussian profile is an inappropriate, unphysical model, and results based upon this model are probably unrealistic.

Based on the fact that a gyroradius-limited profile produces radar echoes that are hundreds to thousands of dBs weaker than are actually observed at 50 and 155 MHz, we conclude that, observationally, plasma drift waves or electron streaming instabilities must be present and responsible for electron density irregularities with spatial wavelengths of three meters and smaller. We suggest that measurement of the intensity of radar backscatter from equatorial spread-F versus radar frequency from HF through UHF will reveal the nature of the physical processes going on in the gradients of large, scintillation-producing structures. It has been suggested that these processes may be important in the dissipation of the large-scale, scintillation-causing irregularities, and an understanding of them will allow quantification of striation decay.

PREFACE

The author thanks Mr. Roland Tsunoda who read this manuscript and made a number of useful suggestions. The author also wishes to thank those members of the SRI support staff who have made the assembly of this report especially easy.

CONTENTS

ILLUSTRATIONS

TABLES

1. INTRODUCTION

It has been known since 1938 that radar echoes could be obtained from the ionosphere near the equator at radar frequencies considerably higher than the local plasma frequency.[1*] The phenomenon has been called equatorial spread-F. In recent years there has been considerable interest in, and study of, equatorial spread-F by means of radar backscatter,[2] satellite-signal scintillation,[3] in-situ satellite probes,[4] air glow,[5] and diagnostics of other kinds. The existence of backscatter echoes at frequencies above the F-region plasma frequency in the HF radar band has been used as an indicator of the presence of ionization irregularities with dimensions of hundreds of meters or more. It is now known that these larger irregularities may also be present when no backscatter is observed. The backscatter has been observed at frequencies as high as 415 MHz.[6,7] All indications are that the radar backscatter is extremely field-aligned, meaning that the radar beam line to the scattering volume must make a 90° angle with respect to the earth's magnetic field in the scattering region.

This report is concerned with understanding the origin of the radar backscatter echoes by attempting to postulate "reasonable," but simple models of the spread-F environment. Though we do not believe we have unambiguously identified the scattering mechanisms, we believe that we have provided substantial "food for thought" for use in guiding either ground-based or altitude-based diagnostics.

1.1 Background

Equatorial spread-F is thought to consist of fluctuations in electron density that are aligned along the earth's magnetic field. The general opinion is that these irregularities result from a generic form of the gradient-drift instability.[8] In the fall of 1977 the Los Alamos

---

* References are listed at the end of the report.

Scientific Laboratory produced a hole by deposition of water vapor into the F region over the island of Kauai in the Hawaiian chain.[9] The LASL experiment was code-named LAGOPEDO. In advance, opinion was that the edges of the ionospheric hole would go unstable by a wind-driven gradient-drift process and could be detected by radar backscatter. Therefore, SRI mounted a radar experiment to attempt to detect these irregularities.[10]

In the planning of the SRI experiment, it was necessary to make a decision concerning radar operating frequency in order to maximize sensitivity to detection of irregularities. The author made a survey of existing experimental literature and found that the spread-F radar scattering demonstrated a very steep frequency dependence between 17 and 55 MHz. At the time, the author decided that a feasible mechanism for producing the radar scattering might be interface reflection between high-density plasma bars (the large size structures several hundred or more meters in dimension) and the low-density background. The problem was how to predict the shape of that gradient and then how to compute the expected interface reflectivity.

The physics of the interface region is poorly understood, but it seemed that under very dynamic circumstances the gradient could steepen to the point where the gyroradius distribution of the dominant ions would prevent additional gradient steepening. We therefore deduced a gradient form for a gyroradius-limited process, computed the reflectivity for this gradient, and found a very steep frequency dependence, which was qualitatively consistent with the HF radar results (consistent in the sense that low system sensitivity could detect spread-F at low HF--for example, at 17 MHz[11]--but very high sensitivity was needed to simultaneously detect spread-F at VHF--for example, at 55 MHz.[12]) Experimental data obtained at UHF frequencies also suggested that plasma drift wave instabilities might be present, but we had no way to predict the presence or magnitude of these.

Based on this theoretical work, an operating band of frequencies was chosen for use during the LASL LAGOPEDO ionospheric depletion experiment. The experiment was carried out; no spread-F echoes were observed due to the plasma hole either by our "spread-F-like" experiment or by standard ionospheric sounder techniques.

Subsequent to these efforts, we discovered that Balsley and Farley had used a similar theoretical approach to predict the ratio of 50-MHz spread-F echoes to incoherent electron backscatter echoes.[13] Further study of their work revealed that their technique predicted more intense echoes than we would predict from our profile. Also, we were able to show that the echoes observed by the ALTAIR radar at 155 and 415 MHz could not be explained by gradient interface reflections of a simple nature and we therefore felt certain that electron drift waves of some sort were probably present when such echoes were observed. Our work laid dormant until very recently, when we resurrected our theoretical predictions and attempted to understand the origin of the differences between our predictions and those made by Balsley and Farley. This report will summarize the results of our efforts.

1.2 Description of Our Spread-F Theoretical Study

In the following sections we describe in detail how we have computed spread-F radar echo strength by several techniques and for several gradient forms for the change in electron density across boundaries between mixing plasmas (i.e., across the edges of large, field-aligned plasma bars). Our first purpose was, as stated above, to understand the differences between our results and those of Balsley and Farley.[13] Our second intent was to determine where gradient interface reflection became so weak with increasing radar frequency that some other mechanism--say, drift-dissipative waves--would have to be invoked to explain the ALTAIR UHF echoes.

We postulated a spread-F environment based on our understanding of the gradient-drift instability as derived from observations of barium clouds. This environment seems to be one consisting of high-density and low-density bars of ionization with, naturally, some kind of transition--or interface gradient--in between. We derived an interface-gradient form between high-electron density inside plasma bars and the exterior low-density plasma based on a diffusive or gyroradius-determined interface. We employed Born approximation scattering for determining the interface

reflectivity and combined this with geometrical optics to derive a total radar cross section.

In order to obtain an idea of the validity of the Born technique as frequency is decreased and approaches the local plasma frequency, we also calculated the interface reflectivity for a second type of profile, the Epstein profile.[14] The Epstein profile is of interest because there exist exact solutions for the interface reflection whether the plasma is overdense or underdense to the radar frequency. Thus, by calculating reflection by Born approximation and by the "exact" technique, a check could be made on the range of validity of the Born approximation.

A third interface profile was used by Balsley and Farley. Their profile was an analytical form, rather than a physically based profile. For reasons that will become clear later, we call this profile a "half-Gaussian" profile. With this form they found rather satisfying agreement between predictions and experiment. This profile led to very intense backscatter compared with either the Epstein or diffusion-controlled profiles. After considerable concern that we were making an error of some sort, we finally suspected that this very large result by Balsley and Farley came about because their profile, the half-Gaussian, was pieced together by two analytical forms. Where the forms joined there is a discontinuity in the second derivative of the profile. Neither the diffusion-determined profile nor the Epstein profile have discontinuities of any order in their derivative. It seemed unlikely to us that nature would produce such a discontinuity.

In order to satisfy ourselves that the intense scattering calculated by Balsley and Farley resulted from the discontinuity in second derivatives where they fit their analytical forms together, we have studied a fourth profile. This fourth profile is called a "raised cosine" profile. It has a discontinuity in the second derivative at the "turn-on" and "turn-off" points. We found that this profile also gives very intense scattering and indeed has the same limiting high-frequency dependence and absolute magnitude as was found for the half-Gaussian profile if the discontinuities in the second derivative were equalized. Though we do not

feel secure that our diffusion-controlled (gyroradius-controlled) profile is physically correct, because we do not understand what nature does in a dynamically mixing plasma, at least the profile does not produce discontinuities in derivatives.

Based on our work, we believe that a measurement of the frequency dependence of radar backscatter from low HF through 415 MHz would be very revealing concerning the nature of plasma processes in a dynamic plasma. Specifically, we believe such an experiment might show the transition between ion-determined gyroradius form and electron oscillations produced by drift-dissipative waves. The experiment would also provide the connection between: (1) the large-scale irregularities that lead to scintillation of satellite signals and their spatial-frequency power spectra as inferred by satellite scintillation, and (2) in-situ probes and the very-short-wavelength irregularities that are responsible for radar backscatter and that possibly play an important role in dissipation of ionospheric irregularities.

1.3 Report Organization

Section 2 of this report describes two generalized models that we hypothesize for use in our spread-F radar scattering study. Section 3 is concerned with the ray-optics (geometrical) approximation for making radar-cross-section calculations. One factor in the radar-cross-section estimate is the interface reflection coefficient between low- and high-density plasma. The radar scattering intensity depends most critically upon the nature of the gradient structure. Section 4 studies four gradients to illuminate various problems in making reflectivity estimates. Section 5 compares various predictions with experimental data, and Section 6 presents the conclusion of our study.

2. MODEL OF ENVIRONMENT USED IN SCATTERING CALCULATIONS

In order to make quantitative estimates of radar backscatter versus frequency, one needs a model of the disturbed equatorial environment. Historically, in radar scattering studies, guesses have been made for a form of the spatial autocorrelation function, and this function then determines the spatial-frequency power spectrum of density fluctuations. The spatial-frequency power spectrum is then used in the Born approximation to make estimates of the backscatter intensity.

Taking a different approach, Balsley and Farley chose a model of electron-density variation in configuration space in order to make their quantitative estimates of the 50-MHz backscatter from equatorial spread-F measured by the Jicamarca radar.[13] Our primary model will likewise be described in configuration space; the model is based on our interpretation of the visible structure seen in up-the-field-line (parallel to the magnetic field line) photographs of striating barium clouds.[15,16] The model also assumes that diffusion- or a gyroradius-determined limiting process shapes the transition profile between high- and low-density plasma.

We make several unproven assumptions in developing our model; however, the point of this effort is not to prove that our model is correct. Our intent is to determine if the model has a useful unifying capability and can also be helpful in making predictions, and can further our understanding of observations of the naturally perturbed, equatorial F region. As we shall see, our model predicts significantly less scattering from spread-F than does the half-Gaussian model.

Again, based on barium-cloud photographs, we assume that the cross-field dimension of these rods may vary between (say) several hundred meters and something less than a kilometer. For ease later in making quantitative calculations, we shall assume that all rods have the same cross-field dimension; we will later choose 330 m. As an alternative, we could choose a distribution in rod radii to match measured in-situ spatial-frequency power spectra at long wavelengths; we save this procedure for a future study.

With very steep edges, of course, the limiting form at small spatial wavelengths for the in-situ, one-dimensional spatial-frequency power spectrum is proportional to the square of the spatial wavelength as λ_s^2 (inversely proportional to the square of the spatial wavenumber as k_s^{-2}). This will be the case for spatial wavelengths down to several tens of meters, for example. At even smaller wavelengths the spatial-frequency power is further diminished in intensity by the finite edge gradient. The very smallest wavelengths observed by radar backscatter (below, probably, several meters) are most likely the result of electron streaming instabilities.

Because the plasma internal energy is thought to be small compared with the magnetic pressure, we assume that the mixing fluids act as generally incompressible fluids. Photographs of barium clouds suggest that the rods that we hypothesize for the F-region model leave behind them, as they convect, a dim wake suggesting some diffusive or edge-ablation mixing. For this reason, we shall assume that less than half the available volume is filled with high-density rods; by symmetry, therefore, also less than half the volume is filled with low-density rods.

The electron density inside the high-density rods will be considered as uniform. In-situ measurements inside barium striations indicate possibly a smooth variation through the rods, but the smooth variation is rather undramatic, in the author's opinion, compared with the steepness of the edges.[17] Thus, at the level of sophistication of our study here, and in the absence of more definitive theoretical or experimental guidance, a uniform internal density seems sufficient.

It will be assumed that the cross-magnetic-field properties of the rods that we have hypothesized remain well correlated parallel to the earth's magnetic field. Quantitatively, we assume that the correlation is excellent for distances of several Fresnel zones for the frequencies that we are studying. For frequencies as low as 15 MHz, this means good correlation at cross-field spatial wavelengths of less than 10 to 15 m over parallel-to-the field distances of (the order of) 5 km for altitudes of 300 km or so. This assumption, which might be supported by theory, is

necessary in order that radar backscatter cross sections can be simply determined by ray theory. Should the parallel-to-the-field correlation distance actually be less than this, but sufficiently longer than the linear dimension of the radar aperture, then we can show that the magnitude of the cross section, in expectation, is not changed. However, it is significantly more difficult to calculate even though the answer is the same.

In order to estimate the total radar cross section, we need to know how many rods traverse each square kilometer perpendicular to the earth's magnetic field. Again, based on our interpretation of barium-cloud photographs, we shall assume that the high-density plasma rods are cylinders. We assume that, by fluid symmetry, low-density rods also exist in equal numbers. We assume that the number of high-density rods is then given as follows:

$$N = \frac{1}{8r^2} \tag{1}$$

where N is the number of rods per square kilometer perpendicular to the earth's magnetic field, and r is the rod radius.

The packing fraction is approximately equal to 40%, which means that about 40% of the area contains high-density rods. By symmetry, then, 40% of the area contains low-density rods and the remaining 20% contains intermediate plasma densities, maybe in the form of tails, or wakes, behind both the high- and low-density rods.

The above parameters describing our model of the equatorial spread-F environment are probably sufficient to make radar-cross-section estimates. Our next task then is to estimate the radar cross section of our model. The results of this effort are divided into two parts. The first part (Section 3) describes the geometric optics part of the calculation. The cross section derived in this way requires a magnitude for the interface reflectivity. Part 2, the derivation of this latter quantity (Section 4), is the most uncertain and is, in fact, the core material of this report. This part of the calculation is described in Section 4.

3. RADAR SCATTERING CROSS SECTION--PART 1: RAY-OPTICS APPROXIMATION

It may be shown that the radar cross section of an individual rod is given by the following:

$$\Sigma = \mathcal{R} \cdot \frac{\pi r R}{(1 - \frac{R}{\rho})(1 + \frac{r}{R})} . \qquad (2)$$

The quantity $\mathcal{R}$ is the edge-interface power reflectivity, the subject of Section 4. If the rod radius, r, is large enough (probably greater than 50 m or so), the quantity $\mathcal{R}$ is the same as that for a plane interface. The quantity R is the range from the radar to the rod.

The quantity ρ is the local radius of curvature of the earth's magnetic field at the scattering specular point. The magnetic-field curvature is such as to cause "focusing." However, as a practical matter, at a range of 300 km on the equator, the "focusing" is only about 15% to 20%--hardly significant, compared with other uncertainties in our modeling. Thus the effect will be ignored from here on.

The validity of Eq. (2) depends on geometric optics, and thus, in concept, requires that coherence distances be comparable to several Fresnel zones, as stated in the description of the environment model in Section 2. If coherence distances, for the spatial wavelengths of concern, are less than this, but are long compared with the linear dimensions of the antenna system, then we can show that the expectation cross section remains unchanged even though this result is not demonstrable by geometric-optics means.

We consider two situations: one in which rod radius, r, is small compared with range R, and the other in which r is very much greater than R. This latter corresponds to a flat layer such as, for example, the normal undisturbed horizontal F layer. The two limiting forms for Eq. (2) are then as follows:

$$\Sigma = \Re\ (\pi r R) \text{ for } r \ll R \qquad \text{(Rod model)} \tag{3}$$

$$\Sigma = \Re\ (\pi R^2) \text{ for } r \gg R \qquad \text{(Flat interface model)} \tag{4}$$

For the rod model, the total, coherent radar cross section is determined by summing the contribution of all rods. The total number observed by the radar is determined by the number of rods per square kilometer perpendicular to the magnetic field [see Eq. (1)] times the cross-magnetic-field area of the radar pulse length and beamwidth. Thus,

$$\Sigma_{coh} \cong \Re\ (\frac{1}{8r^2})(\pi r R)\cdot(\theta_\perp R)\cdot(\frac{c\tau}{2}) \tag{5}$$

where

$\frac{c\tau}{2}$ = Radar pulse length in backscatter

$\theta_\perp$ = Radar beamwidth (radians) perpendicular to the magnetic meridian.

We assert here that Σ_{coh} is most sensitive to the value of $\Re$ which is derived from the interface gradient form. The second term is the geometric part of Eq. (3). The product of the fourth term (cross-field beamwidth) and the fifth term (radar pulse length) give the effective cross-field area of the radar beam.

Collecting terms, Eq. (5) can be reduced to give the following:

$$\Sigma_{coh} = \Re\frac{\pi}{8}\frac{R^2}{r}(\frac{c\tau}{2})\ \theta_\perp \tag{6}$$

The only two parameters that depend quantitatively upon our environment model are $\Re$ and r. Under the assumption that our model concept has some degree of validity, the total cross section depends only weakly on rod dimension r. Based on barium photos and our assumed equivalence of the

barium environment geometry with spread F, r is probably significantly greater than 100 m and significantly smaller than 1000 m. Thus, if we choose a value of 330 m plus or minus a factor of three, the computed total cross section would vary by only ±5 dB, which is hardly significant, as we shall show, compared with our current uncertainty in $\mathcal{R}$.

Woodman and Hoz present their data as a ratio of the coherent-to-incoherent backscatter ratio.[2] To the accuracy that concerns us here, the incoherent-backscatter cross section for a specific radar system is given as follows:

$$\Sigma_{\text{incoh}} \cong \frac{\sigma_t}{2} \cdot \theta_\perp \theta_\parallel R^2 \cdot \frac{c\tau}{2} \cdot \frac{n_o}{2} \tag{7}$$

where $\theta_\parallel$ is the antenna beamwidth parallel to the earth's magnetic field. The quantity σ_t is the Thomson-scattering cross section and is assumed to have a cross section $\approx 10^{-28}$ m^2. We have multiplied by 1/2 under the assumption that only the ionic component contributes. It is also a simple matter to show that, for our model, the average electron density throughout a large volume is $n_o/2$.

The ratio of Eqs. (6) and (7) is

$$P = \frac{\pi}{2} \cdot \frac{1}{\sigma_t} \cdot \frac{\mathcal{R}}{n_o} \cdot \frac{1}{r\theta_\parallel} \quad \text{(rod model)}. \tag{8}$$

This is one relationship that we shall use later when we compare the results of our calculations with the Jicamarca[2] and ALTAIR experiments.[7]

Another comparison ratio to use is that developed by Balsley and Farley, in which they assumed a model of the spread-F environment that was a gradient transition in a single, flat layer. The ratio of the coherent reflection from this layer to the incoherent backscatter is as follows:

$$P_{BF} = \frac{4\pi\mathcal{R}}{\sigma_t(\theta_\perp \theta_\parallel)(\frac{c\tau}{2})n_o} \cdot \tag{9}$$

Another comparison method is to determine the ratio of effective cross section of spread-F to the effective cross section expected from an F-layer overdense reflection. Under the assumption that the F-layer is flat and has perfect reflectivity, we find the following ratio:

$$Q = \Re \cdot \frac{1}{8r} \left(\frac{c\tau}{2}\right) \theta_{\perp} \cdot \qquad (10)$$

From an experimental point of view, sounders that measure from below the ionospheric plasma frequency to substantially above it probably have antenna beamwidths that are substantially broader than we are currently learning is the east-west extent of the spread-F phenomena. Thus the utility of Eq. (10) is not all that clear.

In all of the above, the quantity, $\Re$, the interface reflectivity remains quantitatively undiscussed. We investigate this parameter in the next section.

4. RADAR SCATTERING CROSS SECTION--PART 2: INTERFACE REFLECTIVITY COEFFICIENTS

The shape of the electron density profile from within a plasma bar to outside is the most critical element in the determination of radar scattering cross section. So little is understood about the physics of this profile that the best we can do at this time is to use our intuitive judgement as to physically reasonable profiles. In this section we consider four different profiles. We shall use them for computing radar reflectivity to show how sensitive the radar scattering result is to this profile shape. We show that the Born approximation technique is adequately accurate to frequencies that are as low as twice the plasma frequency. We show that discontinuities in higher-order derivatives of the profile shape lead to radar scattering that we would contend is nonphysical scattering.

4.1 Interface Profile

We consider four profile shapes for transition in electron density across the plasma boundaries. Table 1 lists the analytical form of the four profiles and presents their one-dimensional spatial-frequency power spectra. Table 2 lists the value of the steepest slope, relates profiles by means of steepest slopes, presents asymptotic forms for power spectra at low and high frequencies, and provides other information that will be discussed below. The parameters used in the tables are also described below. We first discuss each profile separately.

4.1.1 Gyroradius- or Diffusion-Controlled Profile

Under quiescent conditions, it is imagined that a sharp plasma gradient will become less steep by cross-magnetic-field diffusion. We also suppose, but cannot prove, that under conditions of dynamic instability growth, the gradient between high-density and low-density

Table 1

PROFILE FORMS AND POWER SPECTRA USED IN THIS STUDY

	(1) Profile Form	(2) Power Spectrum
Diffusive/Gyroradius	$n(x) = n_o[1 + \mathrm{Erf}(\frac{x}{\sigma})]$	$\Phi(k) = \frac{n_o^2 e^{-\frac{(k\sigma)^2}{2}}}{k^2}$
Epstein	$n(x) = \frac{n_o}{1 + e^{-x/\alpha}}$	$\Phi(k) = \frac{n_o^2(\alpha\pi)^2}{\sinh^2(\pi\alpha k)}$
Half-Gaussian	$n(x) = n_o e^{-x/L}$ $x < 0$ $= n_o$ $x > 0$	$g(k) = \frac{n_o}{k}\left\{\sqrt{\pi}(\frac{kL}{2})e^{-(\frac{kL}{2})^2} + j\left[2(\frac{kL}{2})e^{-(\frac{kL}{2})^2}\int_o^{\frac{kL}{2}} e^{t^2}\,dt - 1\right]\right\}$. $\Phi(k) = \lvert g(k)\rvert^2$.
Raised Cosine	$n(x) = \frac{n_o}{2}(1 + \cos\frac{x\pi}{D})$ $\lvert x\rvert < D$ $= 0$ $\lvert x\rvert > D$	$g(k) = \frac{n_o}{k}\left\{\sin kD + \frac{kD}{2}\left[\frac{\sin(kD - \pi)}{(kD - \pi)} + \frac{\sin(kD + \pi)}{(kD + \pi)}\right]\right\}$. $\Phi(k) = [g(k)]^2$.

Table 2

SPECIAL CHARACTERISTICS OF PROFILE FORMS USED IN THIS STUDY

	(1) Steepest Slope	(2) Value of Steepness Parameter for Equal Slopes	(3) Power-Spectrum Limits k→0	(4) Power-Spectrum Limits k-large
Diffusive/Gyroradius	$\frac{n_o}{\sqrt{\pi}\sigma}$	$\sigma = \sigma$	$\frac{n_o^2}{k^2}$	$\Phi(k) = \frac{n_o^2}{k^2} e^{-(\frac{k\sigma}{2})^2}$
Epstein	$\frac{n_o}{4\sigma}$	$\sigma = \frac{\sqrt{\pi}}{4}\sigma$	$\frac{n_o^2}{k^2}$	$\Phi(k) = n_o^2(2\sigma\pi)^2 e^{-2\pi\sigma k}$ $= \frac{n_o^2\pi^3\sigma^2}{4} e^{-\frac{\pi\sqrt{\pi}k\sigma}{2}}$
Half-Gaussian	$\sqrt{\frac{2}{e}}\frac{n_o}{L}$	$L = \sqrt{\frac{2\pi}{e}}\sigma$	$\frac{n_o^2}{k^2}$	$g(k) = \frac{n_o}{k}\left[\frac{2}{(kL)^2} + \frac{2^2(3\cdot1)}{(kL)^4} + \frac{2^3(5\cdot3\cdot1)}{(kL)^6} + \cdots\right]$. $\Phi(k) = \lvert g(k)\rvert^2 = 4\frac{n_o^2}{k^2}\left[\frac{1}{(kL)^4} + \frac{2^2(3\cdot1)}{(kL)^6} + \cdots\right]$.
Raised Cosine	$\frac{\pi}{2D}$	$D = \frac{\pi\sqrt{\pi}\sigma}{2}$ ($D = \frac{\pi}{2}L$ to equalize 2nd derivative discontinuity)	$n_o^2D^2$	$g(k) = \frac{n_o}{k}\sin kD\left[(\frac{\pi}{kD})^2 + (\frac{\pi}{kD})^4 + (\frac{\pi}{kD})^6 + \cdots\right]$. $\Phi(k) = [g(k)]^2$. For equal 2nd-derivative discontinuity $\Phi(k) = 16\frac{n_o^2}{k^2}\sin^2(\frac{\pi}{2}kL)\left[\frac{1}{(kL)^4} + \frac{2\cdot2^2}{(kL)^6} + \cdots\right]$. $\overline{\Phi(k)} = 8\frac{n_o^2}{k^2}\left[\frac{1}{(kL)^4} + \frac{2\cdot2^2}{(kL)^6} + \cdots\right]$.

plasma will steepen until limited by the finite distribution in gyroradius of the ions at the temperature of the plasma. In real, dynamic plasma-growth situations, we suspect that the interface situation may be far more complex, perhaps involving differential ablation of high- and low-temperature ions and possibly alteration of electron profile through streaming-type instabilities. We are currently unprepared to handle the physics of the latter two possibilities.

We model the gyroradius-determined profile as follows:

$$N(x) = \frac{n_o}{2} \left[1 + \text{erf} \left(\frac{x}{\sigma}\right)\right] \tag{11}$$

where

n_o = Electron density inside rods--assumed uniform. Electron density outside rod interface will be taken as being sufficiently low as to be unimportant in interface reflection calculations.

$\sigma = \frac{\sqrt{2k_B mT}}{eB}$

k_B = Boltzman constant

m = Ion mass

T = Ion temperature

e = Electronic charge

B = Magnetic-field strength.

It can be shown that the transition from inside to outside a plasma interface that has suffered cross-field diffusion is also given by the form of Eq. (11) (also Column 1 of Table 1). We hypothesize that under dynamic growing conditions, the gradient steepens until limited by gyroradius distribution; then the parameter σ is related to ion mass,

temperature, etc., as presented above. The computation of this profile for this limit is performed by assuming that there is an abrupt transition (step function) in ion-guiding centers; thus the transition in ion density is determined by the Maxwellian distribution of the individual particles.

After diffusion sets in, the analytical form for the profile remains the same, but the parameter σ becomes larger than that given for the gyroradius limit. Column (2) of Table 1 presents the spatial-frequency power spectrum. The power spectrum involves a parameter

$$k = k_s = \frac{2\pi}{\lambda_s} \tag{12}$$

where λ_s is the spatial wavelength. In this form, k, the spatial wavenumber relates to spatial-frequency content of the profile itself. In radio-wave scattering, a radar wavelength of twice this dimension will probe this spatial wavelength.

In our comparisons of the reflectivity of profiles, we shall equate the steepest slopes. Our rationale is that the steepest slope may be where most of the scattering action takes place. Column (1) of Table 2 presents the steepest slope in terms of the steepness parameter σ for the diffusive profile. In Column (2), we relate the profile steepness parameter for the three profiles to be discussed below to the value of σ used in the diffusive profile when steepest slopes are equalized. Columns (3) and (4) present the asymptotic power spectrum form in the limit of low frequency and high frequency. For the diffusion-controlled profile, the power spectrum increases to infinity at zero wavenumber (infinite spatial wavelength). In the high-frequency limit the power spectrum decays extremely rapidly as a Gaussian form.

4.1.2 Epstein Profile

A second profile that we consider is the Epstein profile. The characteristics of this profile are presented in Row 2 of Table 1. This profile is a nonphysical profile (that is, we believe it is nonphysical for this environment).

The Epstein profile has two important features for our work; the first is that there are no discontinuities in any derivatives of any order, as is the case also for the diffusion-controlled profile and as we think is appropriate in nature. The second important feature is that there exists an exact solution for the reflectivity coefficient with this profile form whether the radar frequency is above or below the plasma's critical frequency. Therefore this profile can be used to make some determinations about the validity of the Born approximation in the expectation that we can use these results to validate the range of correctness for our other calculations that are performed only by Born approximation.

The spatial-frequency power spectra and other parameters for this profile are also given in Table 1 and 2. For the limiting slope at very large k values, we also present the power spectrum using the value σ as related to α when the steepest slopes of the profiles are equalized. The power spectrum at very low spatial frequencies is exactly the same as it is for the diffusive profile. This equal result is expected because any shape transition looks like a sharp, square wave at spatial wavelengths very long compared with the gradient length.

4.1.3 Half-Gaussian Profile

Balsley and Farley had also suggested interface reflectivity as an origin of spread-F.[13] The profile that they used seemed to be chosen for its analytical simplicity and possibly because their Gaussian form seemed similar to a diffusively generated profile. Their form is given in Row 3, Column 1 of Table 1. It is a 1/2 Gaussian matched to a rectangular wave. We would contend that this profile is nonphysical because, at the match between the 1/2 Gaussian and the rectangular wave, only the zeroth and first-order derivatives are equalized. There is an abrupt discontinuity in the second derivative. Table 2 presents the steepest slope in Column 1, and the equivalence to the diffusive steepness profile is presented in Column 2. Column 3 again demonstrates that any transition, however gradual, looks like an abrupt transition

to the very longest wavelengths. Thus, as expected, the spectral form is identical to prior profiles at the very lowest frequencies. The asymptotic form at high spatial frequencies gives a power spectrum that decreases as k^{-6}. This decay with increasing spatial frequency is very much slower than is the decay for the diffusive profile and the Epstein profile.

4.1.4 Raised Cosine

The fourth profile that we consider is a raised cosine. This profile does not vary the electron density from zero to a finite value as do the other profiles. We could have easily used 1/2 a raised cosine and matched it to a rectangular wave in a manner similar to that employed by Balsley and Farley using a Gaussian form. However, our purpose in using this fourth profile is to show that discontinuities in higher-order derivatives lead to scattering signals greater than we would expect nature to give.

The raised-cosine profile has matched zeroth and first-order derivatives at $x = \pm D$. If we had matched a raised cosine to a square wave, then the low-frequency asymptotic limit would also vary as k^{-2}. Since we are interested in derivative discontinuities, the matching to a square wave is not important. Furthermore, the complexity of the mathematics, though tractable, makes analysis tedious and does not teach us anything more in the high-frequency asymptotic limit than does the simple raised cosine.

As will be shown later, in the Born approximation, the scattering intensity depends on the magnitude of the power spectrum at the appropriate wavenumber. We have stated that discontinuities in derivatives lead to scattering; since nature does not normally produce such discontinuities, we allege that profiles that have such discontinuities are nonphysical and the scattering that results is non physical.

In Table 2, last columns of Rows 3 and 4, we present the high-frequency, asymptotic form for the power spectra of the half-Gaussian profile and the raised-cosine profiles. The limiting form of the power spectrum of the raised cosine is also written with D chosen to match each of its two discontinuities to that of the half-Gaussian profile. Thus, on the average, we might expect twice the scattering from the raised-cosine profile as from the half-Gaussian profile. When the $(\sin^2 kD)$ term is averaged, the result is that the magnitude of the power in the dominant term of the series expansion of the power in the raised cosine is exactly twice that in the dominant term in the half-Gaussian profile. We argue, then, that results obtained using the half-Gaussian profile must be viewed with some caution because they are most likely due to discontinuities in derivatives.

4.2 Comparison of Profile Characteristics

Figure 1 presents the plot of the four profiles. To the naked eye they seem quite similar and maybe physically satisfactory. However, the scattering at the radar frequencies of concern in the study will depend very critically on subtle features of the profiles as expressed in their spatial-frequency power spectras. Here lies the difficulty of choosing analytical forms for predictive purposes. As we shall see, the first three profiles, which are of interest to our scattering problem, lead to predictions in radar scattering cross section that vary as much as hundreds of dB from one another at frequencies of interest in our study.

Figure 2 presents a plot of the logarithm of spatial-frequency power versus $k\sigma$ for the first three profiles. The plot shows the asymptotic k^{-2} for low frequencies. It shows also the k^{-6} asymptotic behavior for the half-Gaussian profile. It is quite apparent that the half-Gaussian profile contains significantly more energy at large spatial frequencies than do the other two profiles. The plots were plotted with $\sigma = 1.0$. The slope parameters for the other two profiles were chosen to give the same steepest slope.

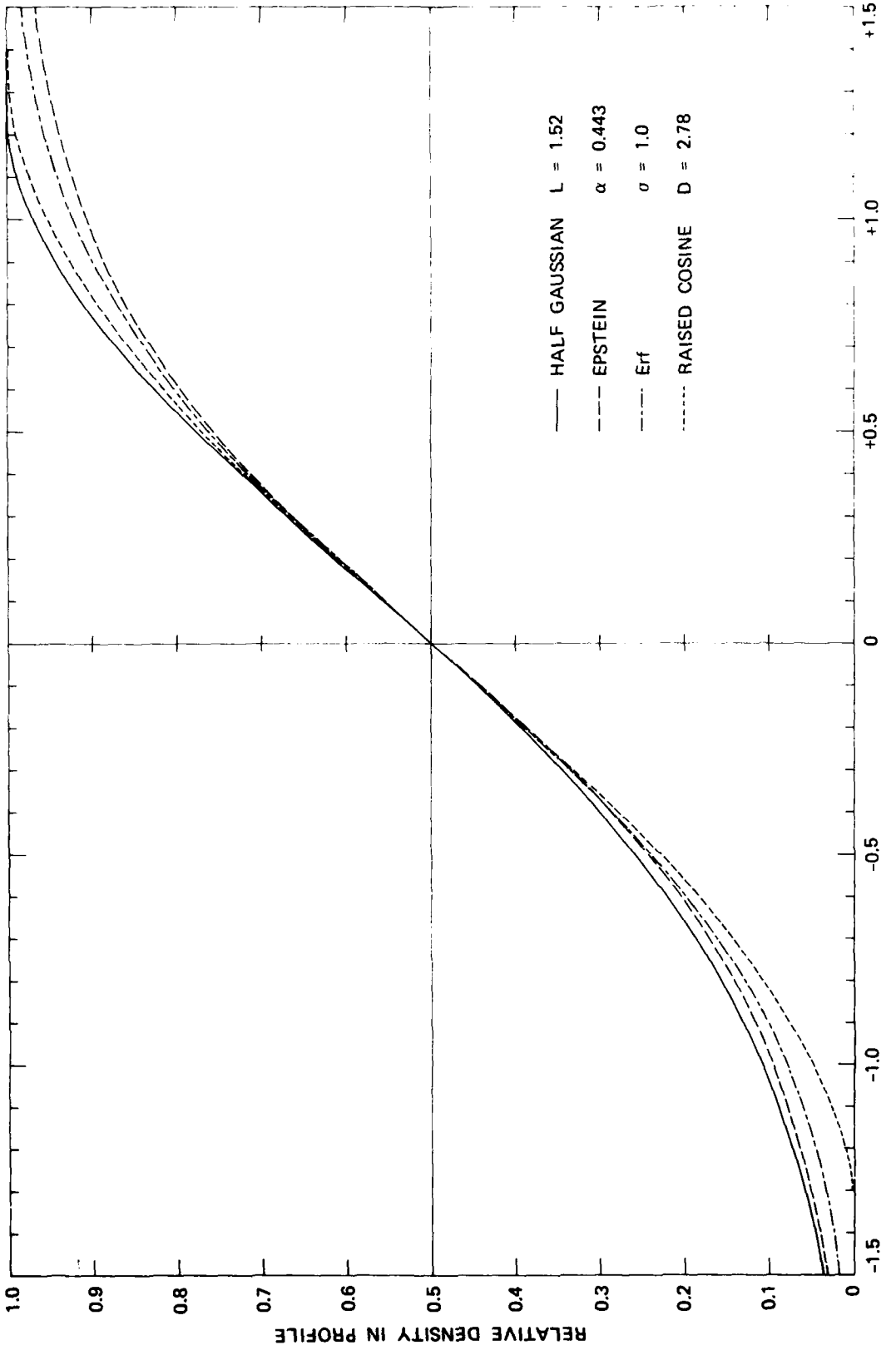

FIGURE 1 PLOTS OF FOUR DENSITY PROFILES USED IN THIS STUDY. Parameters of each profile were chosen to equalize slopes at maximum slope.

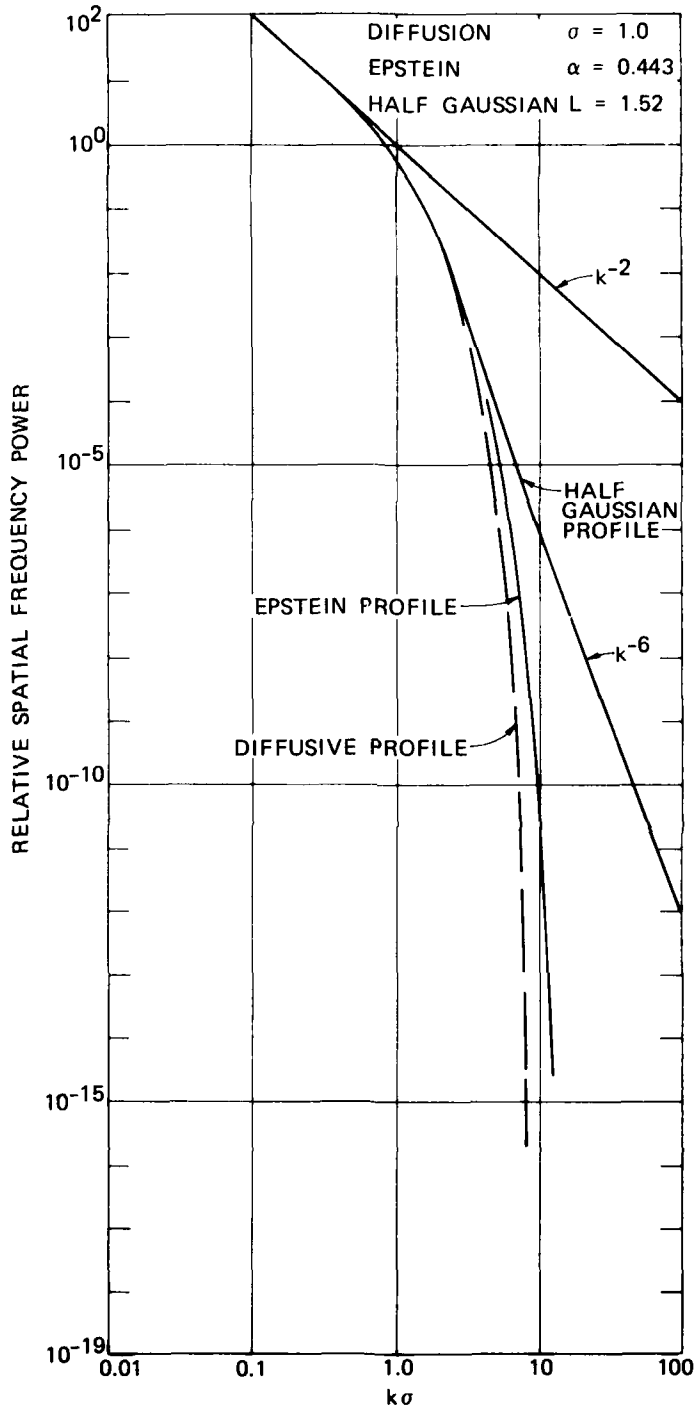

FIGURE 2 LOGARITHM OF RELATIVE SPATIAL FREQUENCY POWER vs. LOGARITHM OF SPATIAL WAVENUMBER (spatial frequency) FOR DIFFUSIVE, EPSTEIN, AND HALF-GAUSSIAN PROFILES

Figure 3 presents the ratio of the half-Gaussian power spectrum to the Epstein spectrum and also the diffusive interface spectrum divided by the Epstein profile spectrum. This plot shows more dramatically how the power at high spatial frequencies diverges for the three profile forms. As we shall see, physical choices for the parameter σ and radar wavenumbers lead to $k\sigma$ values greater than 10, so that the differences do matter very much.

4.3 Reflectivity Characteristics

In this subsection we discuss the techniques used in calculating the reflectivity coefficients. The first technique is essentially Born approximation scattering. The reflectivity coefficient is given as:[13]

$$\mathcal{R} = \left| \frac{-jk_r}{2} \int \frac{\Delta\epsilon(x)}{\epsilon(x)} \, e^{-2jk_r x} \, dx \right|^2 . \tag{13}$$

In this equation the quantity k_r is 2π over the radar wavelength. The quantity ϵ is the dielectric constant as a function of position through the interface, and $\Delta\epsilon$ is the variation as a function of position.

For the Born-approximation scattering to be valid, the radar wave ought to be at a frequency significantly higher than the plasma frequency in the interface. Under this assumption, the reflectivity may be rewritten as

$$\mathcal{R} \cong \left| \frac{-jk_r}{2} \cdot \frac{1}{n_c} \int n(x) e^{-2jk_r x} \, dx \right|^2 . \tag{14}$$

In Eq. (14), the quantity n_c is the electron density necessary for the plasma to be overdense to the radar frequency; $n(x)$ is the electron density as a function of position in the profile. The quantity containing the integral is simply the spatial-frequency power spectrum of the profile form; however, it is evaluated at a spatial wavelength equal to half that of the radar wavelength. Thus we are able to use the power spectra as listed in Tables 1 and 2 for Born-approximation scattering.

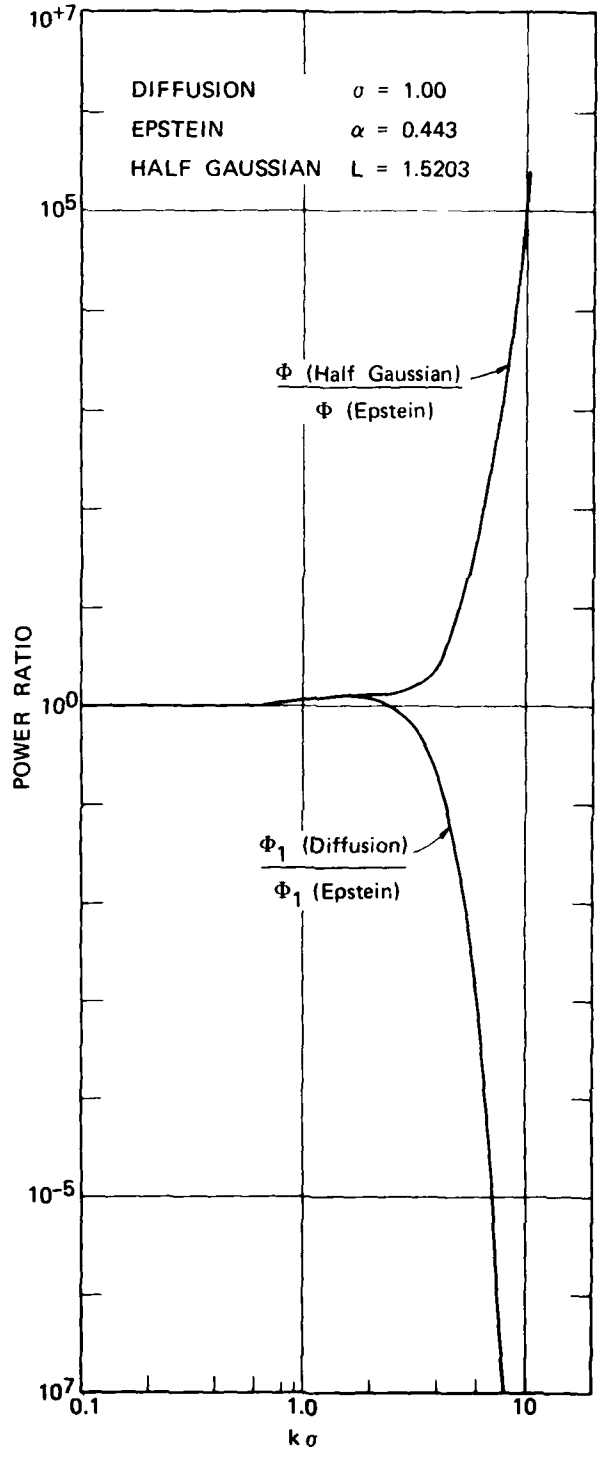

FIGURE 3 RATIO OF SPATIAL FREQUENCY POWER OF DIFFUSIVE AND HALF-GAUSSIAN PROFILES TO THAT OF THE EPSTEIN PROFILE

The coefficient then becomes

$$\Re = \frac{k_r^2}{4n_c^2} \Phi(k = 2k_r) \ . \tag{15}$$

Some electron density profiles are amenable to exact analytical reflectivity determination. This is then a second technique that can be sometimes used. The Epstein profile as given in Table 1 is one of these. The equation for the reflectivity coefficient may be derived from Ref. 14 and is found to be

$$\Re_{Epst.} = \left| \frac{1 - q}{1 + q} \right|^2 \cdot \left| \frac{\Gamma(1 - 2ik_r\alpha)}{\Gamma(1 + 2ik_r\alpha)} \right|^2 \cdot \left| \frac{\Gamma[1 + ik_r\alpha(q + 1)]}{\Gamma[1 + ik_r\alpha(q - 1)]} \right|^2 \tag{16}$$

where

$$q^2 = \varepsilon = 1 - \frac{X}{1 - iZ} = (\mu - i\chi)^2$$

$$k_r = \frac{2\pi}{\lambda_r}$$

λ_r = Radar wavelength

$X = (f_p/f_r)^2$

f_p = Plasma frequency deep inside plasma where the electron density is n_o

f_r = Radar frequency

$Z = f_c/f_r$

f_c = Electron/neutral collision frequency in cycles per second (Hz) [as opposed to ν_c, which is radians per second].

α = Epstein profile gradient steepness parameter.

It can be shown that if the reflectivity coefficient for the Epstein profile is larger than (the order of) 10^{-20}, a very accurate approximation to Eq. (16) is as follows:[18]

$$\mathcal{R} = \left| \frac{1 - q}{1 + q} \right|^2 \exp \left\{ 2 \left[\pi (a - b) - y \log_e \left| \frac{y^2 + a^2}{y^2 + b^2} \right| + 2 \left[b \tan^{-1} \frac{y}{b} - a \tan^{-1} \frac{y}{a} \right] \right] \right\} \qquad (17)$$

with

$$q = (\mu - i\chi)$$

$$y = \frac{1}{2} + k\alpha\chi$$

$$a = k\alpha(\mu - 1)$$

$$b = k\alpha(\mu + 1)$$

Note that since the quantity a may take on negative values, a four-quadrant arctangent routine must be used in evaluating the equation. (Alternatively, one may use the absolute value of a in the terms in the last bracket.)

Figure 4 presents the reflectivity coefficient vs frequency for the Epstein profile as computed by Eq. (17) (meaning analytically exact), and by the Born approximation according to Eq. (15). We see from the figure that the Born approximation reflection coefficient is within a factor of two of the exact procedure for the Epstein profile and for frequencies greater than approximately twice the plasma frequency. We assume but cannot prove that similarly valid ratios would pertain for the diffusive profile and the half-Gaussian profiles. The parameter α was chosen to be 2.50 m; this parameter gives the profile the same maximum slope as a value of σ of 5.66 m in the diffusion-controlled profile. This latter value corresponds to O_{16} ions at a temperature of 1000 K in a 0.3-gauss magnetic field if the profile is gyroradius- rather than diffusion-determined.

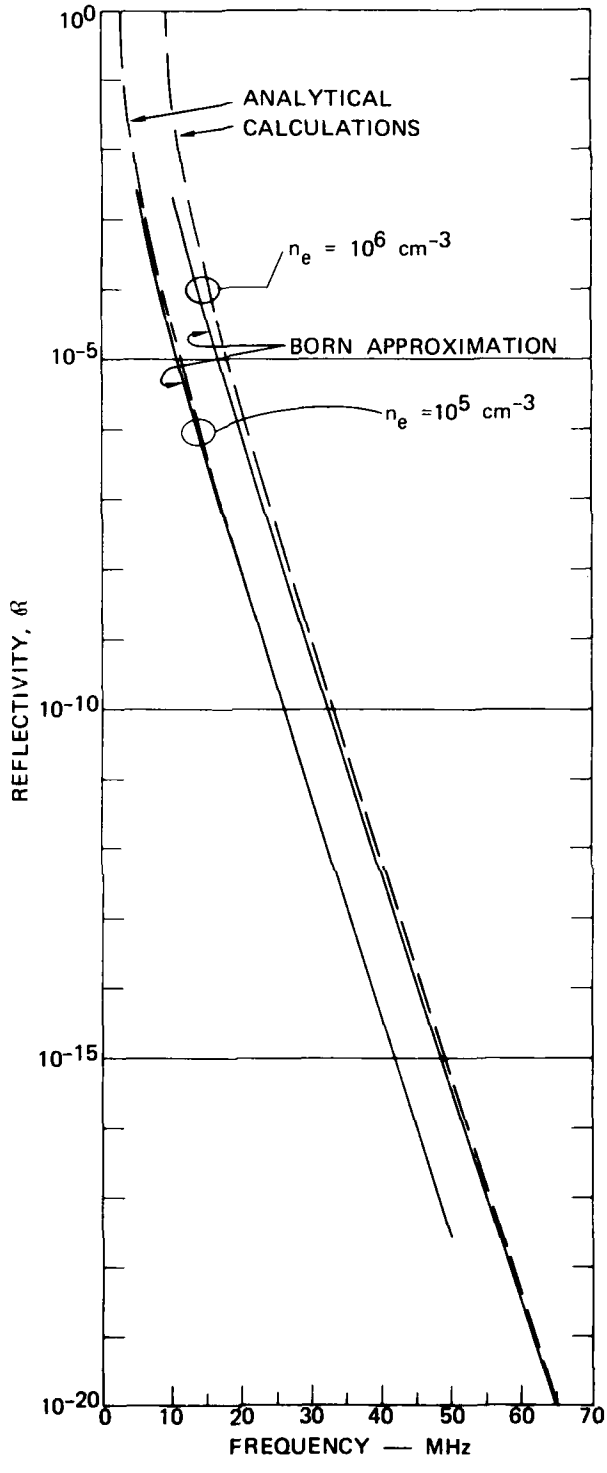

FIGURE 4 INTERFACE REFLECTIVITY vs. RADAR FREQUENCY FOR THE EPSTEIN PROFILE FOR TWO ELECTRON DENSITIES AS CALCULATED BY BOTH EXACT AND BORN APPROXIMATION PROCEDURES

A third means for computing reflectivity is to multiply the Epstein profile reflectivity by the ratio of spatial-frequency power in the diffusion profile divided by spatial-frequency power in the Epstein profile. In a sense, this procedure might be called a "Born approximation correction procedure." In view of the adequacy of the reflection coefficient for the Epstein profile, as computed by the Born approximation, we shall not utilize this third technique.

4.4 Reflectivity Coefficient for the Ionosphere

In this subsection we combine the profile forms presented in Section 4.1 with the Born scattering technique of Section 4.3 to present reflectivity coefficients that may be appropriate to ion density gradients in the ionosphere. We shall consider gradients produced by gyroradius limiting. Therefore the value of σ will be chosen by temperature, ion mass, and magnetic field. Table 3 presents the value of σ for both ionized atomic oxygen and ionized atomic hydrogen for several ionosphere temperatures. Note that if diffusion causes relaxation of the gradient, the effect of this can be simulated by choosing a higher ionospheric temperature.

We have been investigating three profiles that in some sense may simulate ionospheric gradients. (The raised-cosine profile was used only to demonstrate that discontinuities in derivatives lead to non-physical scattering.) Figure 5 presents the reflectivity coefficient versus radar frequency for ionized atomic oxygen at a temperature of 1000 K for the three principal profiles. In all these calculations, we assume that $n_o = 10^{12}$ m^{-3} (a 9-MHz plasma frequency). As we demonstrated in Section 4.3, the Born-approximation scattering probability is adequate for radar frequencies that are more than twice the plasma frequency. This figure shows very dramatically that the scattering expected at high HF and low VHF is very critically dependent upon profile shape. In addition, for all profiles, HF scattering at the low end of the band would be very much more intense then at the high end, which result is consistent with experimental data.

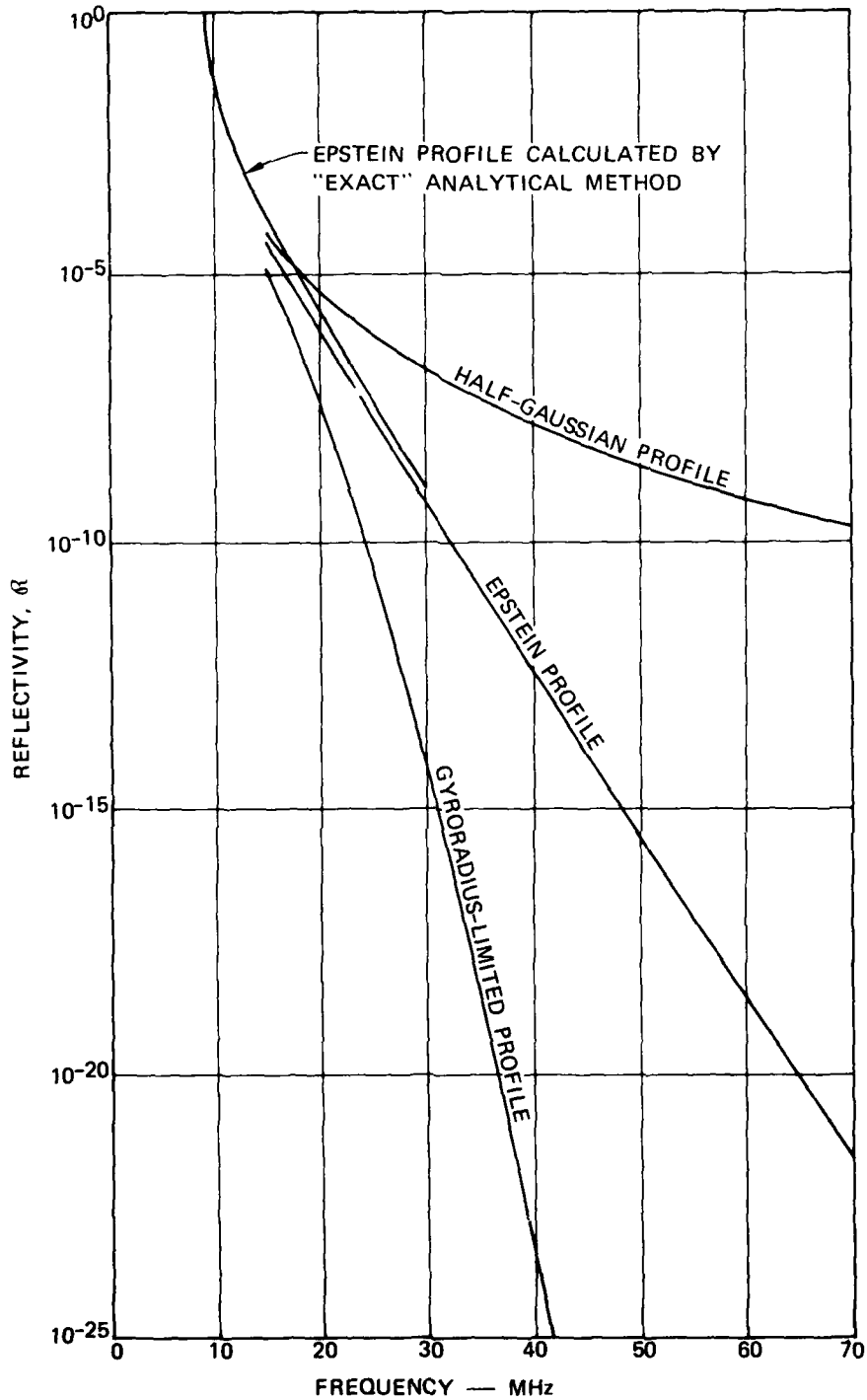

FIGURE 5 INTERFACE REFLECTIVITY vs. RADAR FREQUENCY FOR THE THREE TRANSITION PROFILES WITH AN INTERNAL PLASMA FREQUENCY OF 9 MHz. Slope parameter σ chosen to correspond to gyroradius limited profile of O_{16} ions at 1000° K in 0.3 Gauss magnetic field.

Table 3

VALUES OF THE GYRORADIUS STEEPNESS PARAMETER, σ

(Meters)

Ion \ Temperature (K)	500	1000	2000
H_1^+	1.0	1.42	2.00
O_{16}^+	4.00	5.66	8.00

We have the intuitive feeling that if the plasma gradient is produced simply rather than by a combination of surface ablation and plasma instabilities, then the gyroradius or diffusive profile would be the most reasonable. Figure 6 presents the reflectivity coefficient for oxygen, and temperatures of 500, 1000, and 2000 K for this profile. An electron density of 10^{12} m^{-3} was used (9 MHz plasma frequency). The figure demonstrates that, based on this model, at some frequencies the reflectivity can be an extreme function of temperature.

In the greater heights in the equatorial F region, the ionic constituency changes from ionized atomic oxygen to ionized atomic hydrogen. The reflectivity for ionized atomic hydrogen is presented in Figure 7 for the same three ionospheric temperatures and an electron density of 10^{12} m^{-3}. These data show that the reduced ion mass can lead to such steeper gradients that scattering will be enhanced. It is also interesting that for all three temperatures, and applicable radar frequencies, the frequency dependence is closer to the k^{-2}, "low-k-number" asymptote than the high-k-number limit. For atomic oxygen ions, practical radar frequencies probed principally the high-k-number values.

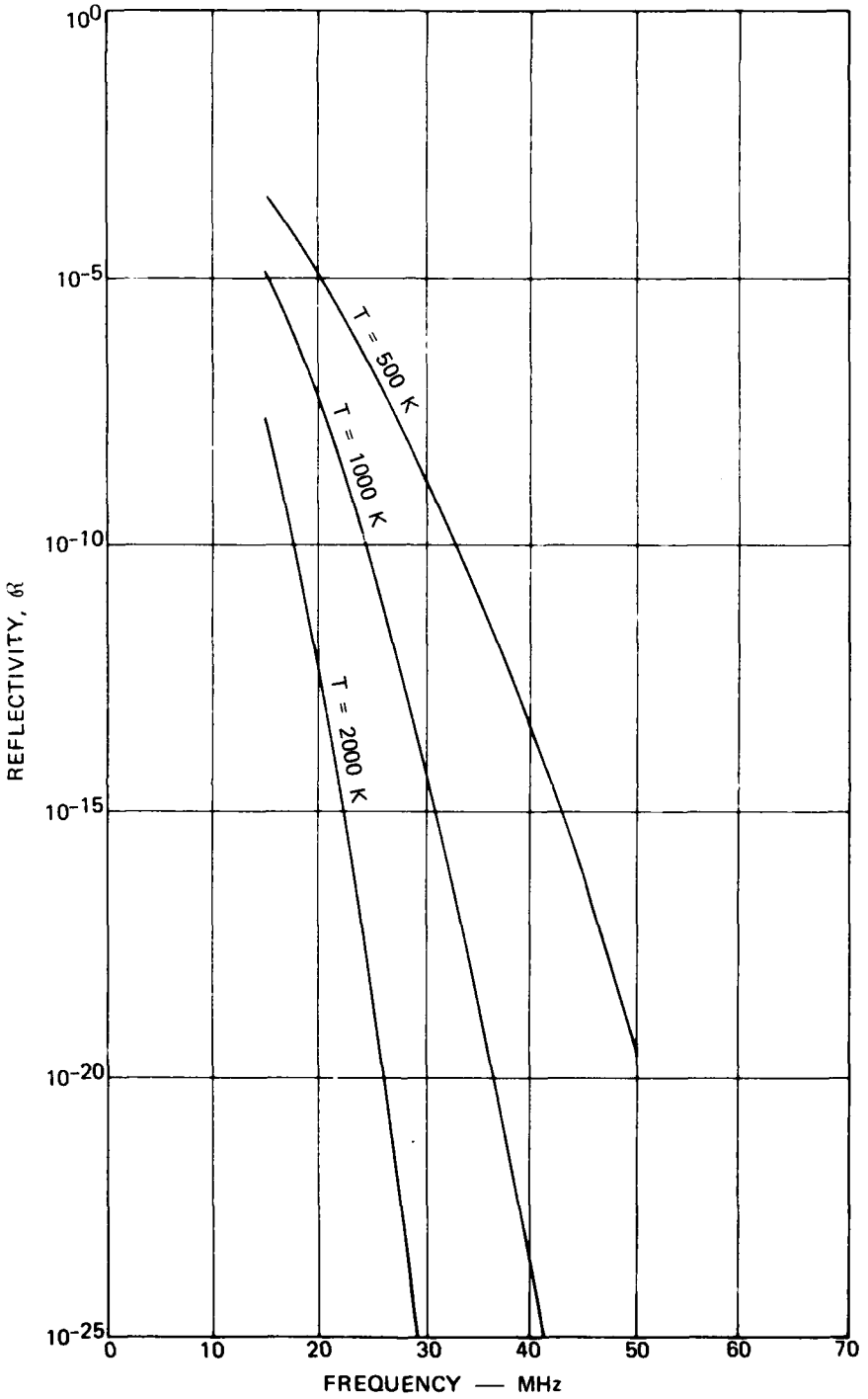

FIGURE 6 INTERFACE REFLECTIVITY vs. RADAR FREQUENCY OF 9 MHz, O_{16} IONS, 0.3 GAUSS MAGNETIC FIELD AND THREE TEMPERATURES AS INDICATED

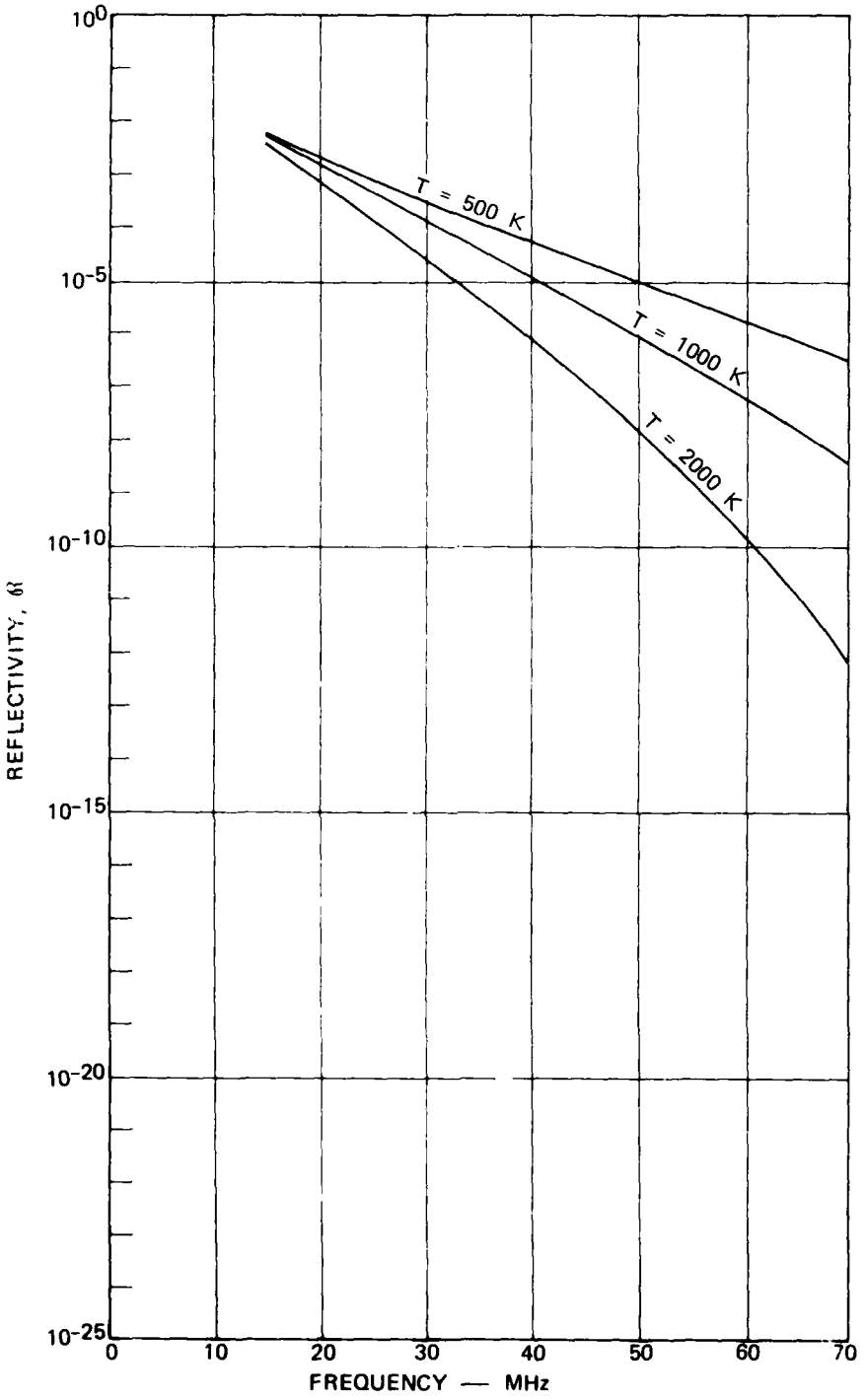

FIGURE 7 INTERFACE REFLECTIVITY vs. RADAR FREQUENCY FOR GYRORADIUS LIMITED PROFILE FOR AN INTERNAL PLASMA FREQUENCY OF 9 MHz, H_1 IONS, 0.3 GAUSS MAGNETIC FIELD, AND THREE TEMPERATURES INDICATED

5. APPLICATION OF CONCEPTS TO EXPERIMENTAL DATA

In this section, the formalisms laid down earlier are used to provide numbers for comparison with experimental data. We shall limit our concern to diffusive control (gyroradius control) profiles and the half-Gaussian profile. Balsley and Farley considered reflectivity from a single transition in a flat ionosphere when they performed their calculations.[13] We shall consider a flat ionospheric transition as well as our rod model.

It can be shown that the ratio of radar cross section for a flat geometry used by Balsley and Farley to the cross section for our rod model is as follows:

$$S = \frac{8r}{(\frac{c\tau}{2})\theta_{\perp}} . \tag{18}$$

In practice, this ratio will be between 10 and 100.

Table 4 presents the ratio, in dB, of coherent scattering to incoherent scattering at 50-MHz frequencies appropriate to the Jicamarca radar. Numerical ratios for both a rod model and a flat interface are presented. The radar and model parameters that we used in the calculations are presented in Table 5.

The data of Table 4 show that if O_{16}^{+} ions are dominant, the half-Gaussian profile, which we contend is nonphysical because of the derivative discontinuity, can produce scattering ratios that are large enough at 50 MHz to explain the Jicamarca data as stated by Balsley and Farley. Inasmuch as we believe the profile is nonphysical, the numberical results, we would argue, are of little direct value. However, the concept of using a shape in configuration space as suggested by Balsley and Farley is extremely valuable.

Table 4

RATIO OF COHERENT TO INCOHERENT SCATTERING FOR JICAMARCA RADAR FOR GYRORADIUS-LIMITED PROFILE AND FOR HALF-GAUSSIAN PROFILE

(dB)

Ion	Temperature (K)	Rod Model		Layer Model	
		Gyroradius-Limited	Half-Gaussian	Gyroradius-Limited	Half-Gaussian
O_{16}^{+}	500	- 38	+ 76	- 27	+ 88
O_{16}^{+}	1000	-191	+ 70	-179	+ 82
O_{16}^{+}	2000	-496	+ 64	-484	+ 76
H_{1}^{+}	500	+104	+105	+116	+116
H_{1}^{+}	1000	+ 95	+ 98	+106	+109
H_{1}^{+}	2000	+ 76	+ 86	+ 89	+101

We believe that the gyroradius profile is more physical than the half-Gaussian profile even if it may also be incorrect. That profile, according to Table 4, does not give sufficient scattering to explain the 50-MHz data. However, even if there were only a small addition of hydrogen ions, and if they behaved separately from the oxygen ions, the gyroradius-limited profile could lead to significant "coherent" backscatter. At higher altitudes where hydrogen does predominate, the gyroradius-limited profile might be adequate.

Table 5

PARAMETERS USED IN COMPUTING DATA PRESENTED IN TABLES 4 AND 6*

Environment	$\sigma_t = 10^{-28}\ m^2$ $n_o = 10^{12}\ m^{-3}$ $r = 330$ m
Jicamarca 50-MHz Radar	$\theta_{\parallel} = \theta_{\perp} = 0.7^\circ$ $(\frac{\sigma\tau}{2}) = 1.5 \cdot 10^4$ m
ALTAIR, 155-MHz Radar	$\theta_{\parallel} \cong 3^\circ$ $\theta_{\perp} \cong 3^\circ$ $(\theta_{\parallel}\,\theta_{\perp})$ term becomes $\pi\left(\frac{\theta_{\parallel}\,\theta_{\perp}}{4}\right)^2$ $\frac{\sigma\tau}{2} = 5 \cdot 10^3$ m

* Results in Tables 4 and 6 were obtained using Eqs. (8) and (9).

Some additional data have recently been obtained at 155 MHz and 415 MHz using the ALTAIR radar.[6,7] Field-aligned echoes have been detected at both frequencies at times when both spread-F and satellite scintillation have been present.

Tsunoda has presented some results at a frequency of 155 MHz.[7] He finds values of the coherent-to-incoherent backscatter ratio often ranging between +20 and +30, but sometimes reaching values as high as +50 dB. Table 5 also presents data for the ALTAIR radar configuration.

Table 6 presents the ratio, in dB, of the coherent to incoherent backscatter for two models of the general environment (rods and a layered transition) and for the gyroradius-limited profile and the half-Gaussian profile.

The results of the table show that the gyroradius-limited profile, even for hydrogen ions, is not capable of explaining the echoes observed by Tsunoda.[7] The half-Gaussian profile, which profile we contend is nonphysical, does produce large scattering ratios.

Table 6

RATIO OF COHERENT TO INCOHERENT SCATTERING FOR
ALTAIR RADAR FOR GYRORADIUS-LIMITED
PROFILE AND FOR HALF-GAUSSIAN PROFILE
(dB)

Ion	Temperature (K)	Rod Model		Layer Model	
		Gyroradius-Limited	Half-Gaussian	Gyroradius-Limited	Half-Gaussian
O_{16}^{+}	500	-thousands	+30	-thousands	+41
O_{16}^{+}	1000	-thousands	+20	-thousands	+31
O_{16}^{+}	2000	-thousands	+18	-thousands	+29
H_{1}^{+}	500	- 3.8	+55	+ 7.3	+66
H_{1}^{+}	1000	- 95	+49	- 84	+60
H_{1}^{+}	2000	-278	+42	-267	+54

6. CONCLUSIONS

This report has described our efforts to understand the nature of field-aligned backscatter echoes from equatorial spread-F. We have hypothesized that radar backscatter in the HF and VHF bands results from interface reflections at steep gradients between high- and low-density plasmas. We have found that using simple, gyroradius-limited models, we cannot explain experimentally observed radar backscatter. As a result we argue that electron streaming instabilities of some sort must be invoked to explain the experimental observations.

In review, we have considered two generalized models of the F-layer. In the first model the environment consists of a number of rods; this model is based on our observations of the results of the gradient-drift instability operating on ionized barium clouds. The second generalized model is that used by Balsley and Farley;[13] it consists of a flat, layered transition from low- to high-density plasma. We have considered four forms for the gradient between low- and high-density plasma.

From the results of calculations that we have presented, we conclude the following:

(1) Based on the one comparison we can make using the Epstein profile, the Born-approximation technique for estimating interface reflectivity is adequately close to the whole-wave ("exact") calculation for our analysis work at frequencies more than twice the local plasma frequency.

(2) Simple gradient scattering leads to a steep frequency dependence of reflectivity, and reflectivity decreases rapidly with increasing frequency. This result, true for all four profiles studied by us, is consistent with experimental trends.

(3) We have not discussed spread-F scattering at frequencies below twice the ionospheric plasma frequency. However, on the basis

of instability calculations by NRL we suspect that ducting up into and back out of bubbles, sometimes called the "whispering-gallery effect," may contribute. We believe that raytracing calculations by some organization able to perform these could shed light on this possibility.

(4) Possibly gradient scattering from a gyroradius-limited interface, as we compute for O_{16}^{+}, contributes to spread-F at frequencies above, say, twice the ionospheric plasma frequency. The inference from our theoretical work is that this gradient scattering decays with increasing radar frequency so very rapidly that the concept probably doesn't apply at 50 MHz and certainly does not apply at 155 MHz. If ionized hydrogen were present as a significant fraction, then, because of its much smaller gyroradius, our gyroradius model could explain even the 50-MHz echoes. The gyroradius-limited profile using hydrogen ions cannot explain the echoes observed by ALTAIR at 155 MHz.

(5) Based on the existence of coherent backscatter echoes at frequencies of 50 MHz and above, and on our feeling that hydrogen ions are not a factor at altitudes where spread-F is often observed, we believe that some kind of streaming instability must be produced probably on the surface of the plasma gradients. We believe that a measurement of the frequency dependence of spread-F backscattering from frequencies as low as the plasma frequency to frequencies above 50 MHz (even to 415 MHz) may provide the data needed to determine the physical processes that go on in the gradients of large, hundred-meter-scale irregularities. Since these physical processes may lead to striation decay, their experimental study and understanding should be of value to the plasma theoretical community studying dissipation of irregularities.

(6) The instabilities that we wish to invoke may generate very steep gradients or may produce a bumpy surface (small-scale wavelengths) in the gradient, both of which could scatter at

50 MHz and higher frequencies. More likely, in our view, streaming instability causes short-wavelength bunching of the electrons, from which radar can scatter, without significantly changing the ion spatial distribution at short spatial wavelengths.

(7) As the plasma dynamics decay, gradients, if they were steep, will soften and radar scattering will decay. However, the gradients may remain steep enough for long periods so that ionized rods of dimensions of hundreds of meters can remain essentially intact and produce satellite signal scintillation when no 50-MHz echoes are simultaneously observed.

(8) Our study of scattering from the half-Gaussian profile with its discontinuity in second derivative and another profile (raised cosine) with two such discontinuities of the same magnitude convince us that the half-Gaussian scattering results are nonphysical. Thus we would argue that the magnitudes of results estimated by Balsley and Farley are fortuitously consistent with Jicamarca results.[13] Despite this, their concept of studying the spread-F radar scattering intensity by working with a plasma profile in configuration space, rather than guessing at a spatial-frequency power spectrum or spatial autocorrelation function, as used to be traditional, has been very useful. The concept has permitted us to apply reasonable, intuitive physical ideas. Thereby it has allowed us to show that, in our interpretation, the observation of field-aligned radar backscatter at VHF and UHF frequencies guarantees that electron streaming instabilities must be responsible for producing the small-scale (3 m and smaller) irregularities.

REFERENCES

1. H. G. Booker and H. W. Wells, "Scattering of Radio Waves by the F-Region of the Ionosphere," Terrest. Magnetism, Vol. 43, p. 249 (1938).

2. R. F. Woodman and C. La Hoz, "Radar Observations of F-Region Equatorial Irregularities," J. Geophys. Res., Vol. 81, p. 5447 (1976).

3. C. L. Rino et al, "Wideband Satellite Observations," DNA 4399F, Contract DNA 001-75-C-0111, SRI International, Menlo Park, CA (June 1977).

4. J. P. McClure, W. B. Hanson, and J. H. Hoffman, "Plasma Bubbles and Irregularities in the Equatorial Ionosphere," J. Geophys. Res., Vol. 82, p. 2650 (1977).

5. E. J. Weber, J. Buchan, R. H. Eathen, and S. B. Mende, "North-South Aligned Equatorial Airglow Depletions," J. Geophys. Res., Vol. 83, p. 712 (1978).

6. D. M. Towle, "Radar Sensing of Ionospheric Irregularities at Wavelengths of 2 Meters and 72 Centimeters," Preprint, 1978.

7. R. Tsunoda, "ALTAIR: An Incoherent Scatter Radar for Equatorial Spread-F Studies," DNA 4538T, Contract DNA 001-77-C-0220, SRI International, Menlo Park, CA (January 1978).

8. S. L. Ossakow and P. K. Chaturvedi, "Morphological Studies of Rising Equatorial Spread F Bubbles," J. Geophys. Res., Vol. 83, pp. 2085-2090 (May 1, 1978).

9. M. B. Pongratz, G. M. Smith, C. D. Sutherland, and J. Zinn, "Lagopedo--Two F-Region Ionospheric Depletion Experiments," preprint of article, University of California, Los Alamos Scientific Laboratory, Los Alamos, NM (December 1977).

10. W. G. Chesnut, G. N. Oetzel, and A. McKinley, "A Search by Radar Backscatter for Irregularities Produced by the Lagopedo F-Region Electron Depletion Releases," DNA 4537F, Contract DNA 001-77-C-0267, SRI International, Menlo Park, CA (February 1978).

11. B. R. Clemesha, "An Investigation of the Irregularities in the F-Region Associated with Equatorial Type Spread-F," J. Atmos. Terr. Phys., Vol. 26, pp. 91-112 (1964).

12. B. B. Balsley, G. Haerendel, and R. A. Greenwald, "Equatorial Spread F: Recent Observations and a New Interpretation," J. Geophys. Res., Vol. 77, No. 28, p. 5625-5628 (October 1972).

13. B. B. Balsley and D. T. Farley, "Partial Reflections: A Source of Weak VHF Equatorial Spread-F Echoes," J. Geophys. Res., Vol. 80, p. 4735 (1975).

14. K. G. Budden, Radio Waves in the Ionosphere, Section 17, Cambridge University Press, Cambridge (1961).

15. T. N. Davis et al., "Observations of the Development of Striations in Large Barium Ion Clouds," Planet. Space Sci., Vol. 22, No. 1, pp. 67-78 (January 1974).

16. W. G. Chesnut, working document, photographs of Events Spruce II and Redwood, Stanford Research Institute, Menlo Park, CA (1971).

17. K. L. Baker et al. (7 authors), "Electron Density Structure in Barium Clouds - Measurements and Interpretation," DNA 4561F, DNA 001-76-C-278, Utah State University, Logan, Utah (February 1978).

18. W. G. Chesnut, "Radar Reflection Coefficients from a Plasma Gradient with Collisions," DNA Report DASA 2185, Contract DA-49-146-XZ-184, Stanford Research Institute, Menlo Park, CA (October 1968).

DISTRIBUTION LIST

DEPARTMENT OF DEFENSE

Assistant to the Secretary of Defense
Atomic Energy
ATTN: Executive Assistant

Command & Control Technical Center
ATTN: C-650

Defense Advanced Rsch. Proj. Agency
ATTN: TIO

Defense Communications Agency
ATTN: Code 480
ATTN: Code R1033, M. Raffensperger
ATTN: Code 101B
ATTN: Code 810, J. Barna

Defense Communications Engineer Center
ATTN: Code R820
ATTN: Code R410, J. McLean

Defense Nuclear Agency
ATTN: DDST
ATTN: RAAE
ATTN: STVL
4 cy ATTN: TITL

Defense Technical Information Center
12 cy ATTN: DD

Field Command
Defense Nuclear Agency
ATTN: FCPR

Field Command
Defense Nuclear Agency
Livermore Division
ATTN: FCPRL

Interservice Nuclear Weapons School
ATTN: TTV

Joint Chiefs of Staff
ATTN: C3S, Evaluation Office

Joint Strat. Tgt. Planning Staff
ATTN: JLTW-2

National Security Agency
ATTN: R-52, J. Skillman

NATO School (SHAPE)
ATTN: U.S. Documents Officer

Undersecretary of Def. for Rsch. & Engrg.
ATTN: Strategic & Space Systems (OS)

WWMCCS System Engineering Org.
ATTN: R. Crawford

DEPARTMENT OF THE ARMY

BMD Advanced Technology Center
Department of the Army
ATTN: ATC-T, M. Capps

DEPARTMENT OF THE ARMY (Continued)

Harry Diamond Laboratories
Department of the Army
ATTN: DELHD-N-P, F. Wimenitz
ATTN: DELHD-I-TL, M. Weiner
2 cy ATTN: DELHD-N-P

U.S. Army Comm-Elec. Engrg. Instal. Agency
ATTN: CCC-EMEO-PED, G. Lane

U.S. Army Foreign Science & Tech. Ctr.
ATTN: DRXST-SD

U.S. Army Satellite Comm. Agency
ATTN: Document Control

U.S. Army TRADOC Systems Analysis Activity
ATTN: ATAA-PL

DEPARTMENT OF THE NAVY

Naval Electronic Systems Command
ATTN: PME 106-4, S. Kearney
ATTN: Code 501A
ATTN: PME 106-13, T. Griffin

Naval Intelligence Support Ctr.
ATTN: NISC-50

Naval Ocean Systems Center
ATTN: Code 532

Naval Research Laboratory
ATTN: Code 6700, T. Coffey
ATTN: Code 7500, B. Wald
ATTN: Code 7175, J. Johnson
ATTN: Code 7580

Naval Surface Weapons Center
ATTN: Code F31

Strategic Systems Project Office
Department of the Navy
ATTN: NSP-2722, F. Wimberly
ATTN: NSP-2141

DEPARTMENT OF THE AIR FORCE

Air Force Avionics Laboratory
ATTN: AAD, A. Johnson

Air Force Geophysics Laboratory
ATTN: PHP, J. Mullen
ATTN: OPR-1, J. Ulwick
ATTN: PHP, J. Aarons
ATTN: PHI, J. Buchau

Air Force Weapons Laboratory
Air Force Systems Command
ATTN: SUL
ATTN: DYC

Ballistic Missile Office
Air Force Systems Command
ATTN: MNNL, S. Kennedy

DEPARTMENT OF THE AIR FORCE (Continued)

Foreign Technology Division
Air Force Systems Command
ATTN: NIIS, Library

Headquarters Space Division
Air Force Systems Command
ATTN: SKA, M. Clavin

Rome Air Development Center
Air Force Systems Command
ATTN: TSLD

Strategic Air Command
Department of the Air Force
ATTN: XPFS, B. Stephan
ATTN: ADWATE, B. Bauer
ATTN: NRT

Air Force Technical Applications Center
ATTN: TN

DEPARTMENT OF ENERGY CONTRACTORS

EG&G, Inc.
Los Alamos Division
ATTN: Document Control for D. Wright
ATTN: Document Control for J. Colvin

Lawrence Livermore Laboratory
ATTN: Document Control for Tech. Info. Dept.

Los Alamos Scientific Laboratory
ATTN: Document Control for R. Jeffries
ATTN: Document Control for J. Wolcott
ATTN: Document Control for MS 664, J. Zinn

Sandia Laboratories
ATTN: Document Control for D. Dahlgren
ATTN: Document Control for Org. 4241, T. Wright
ATTN: Document Control for Org. 1250, W. Brown

OTHER GOVERNMENT AGENCIES

Central Intelligence Agency
ATTN: OSI/PSTD

Institute for Telecommunications Sciences
ATTN: W. Utlaut

DEPARTMENT OF DEFENSE CONTRACTORS

Aerospace Corp.
ATTN: N. Stockwell
ATTN: I. Garfunkel
ATTN: R. Slaughter

University of Alaska
ATTN: Technical Library

Berkeley Research Associates, Inc.
ATTN: J. Workman

Boeing Co.
ATTN: D. Murray

Charles Stark Draper Lab., Inc.
ATTN: J. Gilmore
ATTN: D. Cox

DEPARTMENT OF DEFENSE CONTRACTORS (Continued)

Computer Sciences Corp.
ATTN: J. Spoor
ATTN: C. Nail

Cornell University
ATTN: D. Farley, Jr.

Electrospace Systems, Inc.
ATTN: P. Phillips

ESL, Inc.
ATTN: C. Prettie
ATTN: J. Marshall

General Electric Co.
ATTN: F. Reibert

General Electric Co.—TEMPO
ATTN: DASIAC
ATTN: W. Knapp

General Research Corp.
ATTN: J. Garbarino
ATTN: J. Ise, Jr.

University of Illinois
ATTN: Security Supervisor for K. Yeh

Institute for Defense Analyses
ATTN: E. Bauer

International Tel. & Telegraph Corp.
ATTN: Technical Library

JAYCOR
ATTN: S. Goldman

Johns Hopkins University
ATTN: T. Potemra
ATTN: Document Librarian

Kaman Sciences Corp.
ATTN: T. Meagher

Linkabit Corp.
ATTN: I. Jacobs

University of Lowell Rsch. Foundation
ATTN: K. Bibl

M.I.T. Lincoln Lab.
ATTN: D. Towle

McDonnell Douglas Corp.
ATTN: Technical Library Services

Mission Research Corp.
ATTN: R. Bogusch
ATTN: R. Hendrick
ATTN: R. Kilb
ATTN: F. Fajen
ATTN: D. Sappenfield

Mitre Corp.
ATTN: W. Hall
ATTN: W. Foster
ATTN: J. Wheeler

DEPARTMENT OF DEFENSE CONTRACTORS (Continued)

R & D Associates
ATTN: B. Gabbard
ATTN: R. Lelevier
ATTN: M. Gantsweg
ATTN: W. Karzas
ATTN: C. MacDonald

Rand Corp.
ATTN: C. Crain
ATTN: E. Bedrozian

Science Applications, Inc.
ATTN: L. Linson
ATTN: D. Sachs
ATTN: D. Hamlin

DEPARTMENT OF DEFENSE CONTRACTORS (Continued)

SRI International
ATTN: R. Leadabrand
ATTN: C. Rino
ATTN: V. Gonzales
ATTN: R. Hake, Jr.
ATTN: D. McDaniels
3 cy ATTN: W. Chesnut

Technology International Corp.
ATTN: W. Boquist